4/11

Precipitate size distribution in alloys with and without lattice misfit

Richard Weinkamer[1], Himadri Gupta[2], Joel L. Lebowitz[2], and Peter Fratzl[1]

[1] *Erich Schmid Institut für Materialwissenschaft, Österreichische Akademie der Wissenschaften & Institut für Metallphysik, Montanuniversität Leoben, Jahnstraße 12, A-8700 Leoben, Austria*

[2] *Departments of Mathematics and Physics, Rutgers University, Busch Campus, New Brunswick, 08903 New Jersey, USA*

(draft, September 6, 2000)

---

[70] Dedicated to Professor Dr. rer. nat. Dr. h.c. Hein Peter Stüwe on the occasion of his 70th birthday

Abstract

We investigate, via three-dimensional atomistic computer simulations, the influence of a lattice misfit between precipitates and matrix on the precipitate size distribution during phase separation in a binary alloy. The elastic interactions are modeled by springs connecting nearest neighbor atoms. The difference in size between the two species of atoms, specified by the misfit parameter δ, leads to effective long range interactions. Performing simulations with five different values of δ we find a broadening of the scaled precipitate size distribution for $\delta > 0.5\%$ in comparison with the case of no misfit. Additionally, the size of the largest precipitate in the system increases with increasing misfit. We also observe a percolated network-like precipitate structure for a concentration of solute atoms as low as $c_A = 0.2$ at large misfit. We interpret these effects as due to an increased tendency of the precipitates to coalesce, which is caused by their non-spherical shape, their alignment along the $\langle 100 \rangle$-directions and their regular arrangement.

64.60.Qb, 05.70.Fh, 64.75.+g, 81.30.Mh, 02.70.Lq

Zusammenfassung

Mittels dreidimensionaler atomistischer Computersimulationen wurde die Größenverteilung von Ausscheidungen in einer binären Legierung in Abhängigkeit von der Gitterfehlpassung studiert. Die elastischen Wechselwirkungen im Gitter wurden durch Federn zwischen Nächsten-Nachbaratomen modelliert. Die Gitterfehlpassung, beschrieben durch einen Parameter δ, wurde durch eine unterschiedliche Größe der beiden Atomsorten berücksichtigt, was zu effektiven, langreichweitigen Paarwechselwirkungen im Gitter führt. Simulationen mit fünf verschiedenen Werten für δ ergaben eine Verbreiterung der skalierten Größenverteilung der Ausscheidungen für $\delta > 0.5$. Darüber hinaus befand sich mit wachsender Fehlpassung ein immer höherer Anteil der ausgeschiedenen Atome in der größten Ausscheidung. Bei einer Konzentration von 20% an Ausscheidungsatomen bildete sich bei höherem δ sogar eine perkolierte, netzwerkartige Struktur anstatt isolierter Ausscheidungen. Wir führen diese Effekte auf eine häufige Verschmelzung von Ausscheidungen zurück, was sich durch ihre auf Grund der Fehlpassung veränderte Form und Anordnung erklären lässt.

I. INTRODUCTION

At late stages of a coherent precipitation process, the total amount of interface between precipitates and matrix is typically reduced via a coarsening process with large precipitates growing at the expense of smaller ones [1–3]. The mechanism underlying coarsening was elucidated in the papers of Lifshitz and Slyozov [4] and Wagner [5] (LSW). Their theory predicts that at late times t the precipitate size distribution, $f(R,t)$, takes a scaling form. $f(R,t) = g(R/\bar{R})/\bar{R}$, where $g(\rho)$ is a function independent of time and the mean precipitate size $\bar{R}$ is proportional to the cube root of the time, $\bar{R} \propto t^{1/3}$. Two important assumptions of the LSW-theory are: 1) the neglect of the influence of neighboring precipitates on the coarsening rate so the theory is valid only in the limit of vanishing volume fraction c_A of the precipitate phase. 2) the theory does not consider elastic coherency strains caused by a difference in lattice parameter or elastic constants between precipitates and matrix. More realistic models of coarsening, which abandoned one or the other of these LSW-assumptions, left the results cited above essentially unaltered. Allowing a finite volume fraction of precipitate phase resulted only in a slightly broadened, but still time-independent scaled precipitate size distribution [6–12]. Recently performed experiments under microgravity conditions corroborated these predictions [13]. Similarly, moderate elastic stress should not affect the qualitative predictions either, as long as the volume fraction of precipitate phase stays small [14]. The situation changes however when account is taken of both elastic misfit interactions and finite volume fraction effects [15]. Experimental and computational investigations provide examples of a slowing down of the coarsening process at later stages [16]. This paper addresses the question of the effect of a lattice misfit on the precipitation process using computer simulations of a simple model [17,18]. In particular, we study the precipitate size distribution as a function of misfit and volume fraction of precipitates. A narrower scaled size distribution has been predicted [19] as a consequence of an inverse coarsening process [20], wherein small precipitates grow at the expense of larger ones to minimize the elastic misfit energy. Although such a narrowing was observed in some systems, e.g. Ni-Cu-Si

alloys [21], there are indications from model calculations [22] that a broadening may also take place. Our model considers only an elastic misfit between the phases, but no dislocations. In real systems of course, misfit dislocations are expected to develop at the interface in the presence of large misfit. Nevertheless, Monte Carlo simulations employing this model have proven successful in studies of the influence of internal and external stress on phase separation in two dimensions [17,23] and recently also in three dimensions [24,18].

II. THE MODEL

In our model of a binary alloy A and B atoms occupy the N sites of a coherent *fcc* lattice with periodic boundary conditions. Atoms on nearest neighbor sites are assumed to interact "chemically", with like atoms attracting one another leading to phase separation. The elastic interactions due to the size mismatch between A and B atoms, are modeled by connecting nearest neighbor atoms with springs having a longitudinal and two transverse spring constants. The spring constants are assumed to be independent of the type of atoms they are connecting, so the equilibrium spacing between the centers of a pair of atoms depends on their sizes. We refer the reader to [17] for a detailed description. The total energy of the system, $\mathcal{H}$, is then a function of the lattice configuration of the atoms, which is described by a spin variable $\gamma(\mathbf{r})$ taking the value $\gamma(\mathbf{r}) = +\mathbf{1}$ if there is an A atom at site $\mathbf{r}$ and $\gamma(\mathbf{r}) = -\mathbf{1}$ if there is an B atom at this site, and also a function of their displacement, $u(\mathbf{r})$, from their lattice reference site $\mathbf{r}$. Since the atoms in a real alloy relax to their elastic equilibrium position much faster than they diffuse to a new position, we assume the system is always in elastic equilibrium obtained by minimizing $\mathcal{H}$ over the atomic displacements $u(\mathbf{r})$. The resulting Hamiltonian $\mathcal{H}$ which depends only on the atomic configuration, is given in a compact form in Fourier space as [25–27,17]

$$\mathcal{H} = \frac{1}{2N} \sum_{\mathbf{k}} \Psi(\mathbf{k}) \mid \tilde{\gamma}(\mathbf{k}) \mid^2, \tag{1}$$

where the summation extends over the first Brillouin zone and $\tilde{\gamma}(\mathbf{k})$ denotes the Fourier transform of $\gamma(\mathbf{r})$. Translated to real space, this corresponds to a system with anisotropic

long range pair interactions. The functional form of $\Psi(\mathbf{k})$ and details on the model can be found in reference [18].

All parameters of our microscopic model, which are contained in the function $\Psi(\mathbf{k})$, are experimentally accessible. The spring constants of the connecting springs were chosen according the Born-von Karman parameters of copper [28]. This results in a negative elastic anisotropy of the model, i.e. the elastically soft directions are the $\langle 100 \rangle$-directions. The size difference between A and B atoms determines the lattice misfit, $\delta = (a_A - a_B)/a_A$, where a_A and a_B are the lattice parameters of pure A and pure B phases.

We performed simulations with five different lattice misfits, $\delta = 0\%$ (no misfit), and $\delta = 0.25\%$, 0.5%, 0.75% and 1%. The model fcc lattice comprised 48^3 cubic unit cells, i.e. the number of atoms was $N = 442368$. Two different concentrations of solute A atoms, $c_A = 0.1$ and $c_A = 0.2$ were considered. The simulation temperature was $T = 0.51T_0$, T_0 being the critical temperature of a nearest neighbor Ising model on an fcc lattice. The atomic configurations evolved in time by a standard Metropolis algorithm with Kawasaki exchange dynamics of nearest neighbor atoms [29]. The simulation time unit is one Monte Carlo step (MCS), i.e. one attempted exchange per lattice site. All simulations were carried out up to 6000 MCS starting from an initial quenched state corresponding to a random mixture of A and B atoms.

III. RESULTS AND DISCUSSION

Figure 1 demonstrates the influence of an elastic misfit between matrix and precipitates on the microstructure. The three plots correspond to three different misfits ($\delta = 0\%$, 0.5% and 1%, respectively) increasing from left to right. The two-dimensional plots of the three-dimensional system were obtained by averaging the concentration of solute A atoms along lines normal to the plotting plane and therefore can be read like X-ray transmission micrographs. The salient feature of the plots are an increasing regularity in the spacing between precipitates with increasing misfit. Also the shape of the precipitates evolve from a "blob"-

like appearance into a more needle-like morphology. The plot in the middle corresponding to the case of a small misfit combines features of the plots to the left and right: the blurry structure, but also some alignment along the elastically soft ⟨100⟩-directions.

Figure 2 shows the percentage of solute A atoms contained in the largest cluster, n_{max}, plotted as a function of time. A cluster was defined as a set of A atoms, all connected by nearest neighbor bonds. At the concentration $c_A = 0.1$ all largest clusters start out very small and n_{max} grows more rapidly when the lattice misfit increases. For the largest misfits it reaches as much as 13% by the end of the run. Evaluation of the mean precipitate size, however, showed that that the larger values of n_{max} are not the result of an overall increased coarsening rate for large misfit [18]. The behavior is dramatically different in the model alloy with the higher content of A atoms (Fig. 2, right). Already from the very beginning almost all A atoms are contained in the largest cluster. This is due to percolation which occurs in a random solid solution on an fcc lattice above the concentration threshold $c_{fcc}^{random} = 0.198$ [30]. Without elastic misfit, condensation into precipitates quickly leads to a break-up into individual droplets, the largest containing less than 10% of the A atoms. At a misfit value greater than 0.5%, however, the condensation does not lead to individual precipitates and a percolated structure, perpendicularly interconnected, (such as in Fig. 1, right) develops. which comprises almost all A atoms ($n_{max} \approx 100\%$). It is quite remarkable that for the same concentration and temperature, there is either the occurrence of isolated precipitates or a percolated microstructure depending on the misfit, which suggests that the dynamic percolation transition [31,32] depends on the misfit.

With the definition of a cluster given above, we determined a precipitate size distribution $f(n)$, where f denotes the number of clusters comprising n atoms. n or equivalently the volume of a precipitate, is proportional to R^3, where R defines an effective radius only since the precipitates are not spherical. The mean effective radius $\bar{R}$ is then defined, for small values of the concentration, as

$$\bar{R} = \frac{\sum_{n \geq n_0} n^{1/3} f(n)}{\sum_{n \geq n_0} f(n)} \tag{2}$$

where monomers and other clusters smaller than $n_0 = 10$ were discarded, because they can be considered as being part of the matrix. In Figure 3 the number of clusters of a given size, g, is plotted versus the scaled variable $\rho \equiv R/\bar{R}$ for $c_A = 0.1$ and varying misfit. The scaled precipitate size distribution $g(\rho)$ is normalized so that $\sum g(\rho) = 1$. To improve statistics, we averaged $g(\rho)$ over intervals of length $\Delta\rho = 0.2$, where the data points in Figure 3 mark the middle of these intervals. Since we are interested in late time distributions, we determined $g(\rho)$ after 3000 MCS and then every 500 MCS, i.e. seven independent distributions were obtained for each misfit. The data points and error bars in Figure 3 correspond to the mean value and the standard deviations of the mean of these data. Despite the poor statistics due to the small system size, an influence of the lattice misfit on the scaled precipitate size distribution can be observed. There is a broadening of $g(\rho)$ for large misfit, $\delta > 0.5$, compared to the distributions for smaller misfits indicating that the system contains larger clusters when elastic interactions are more dominant, which is consistent with Fig. 2. A strong difference in $g(\rho)$ from the scaled precipitate size distribution derived from the LSW-theory can be observed for all values of δ. This is consistent with the LSW-function being too narrow compared to those observed at finite volume fraction [6]. Moreover, there is a shift to the left of the maximum position of our simulated $g(\rho)$ as compared to the LSW-result. This may be ascribed to our times not being long enough. To test this, we have performed simulations on a larger system and longer times in the case of no misfit, which revealed a slight shift of the maximum of $g(\rho)$ to the right for longer times, a result also observed experimentally [13].

As already noted for $c_A = 0.2$ a single cluster contains almost all A atoms for large misfits (Fig. 2b, right). Nevertheless, this does not mean that all atoms have assembled into a single compact precipitate. In fact, looking at Figure 1 suggests a rather continuous transition with increasing anisotropy in cluster shape, orientation and position. For large misfit (Fig. 1a) precipitates elongated along $\langle 100 \rangle$-directions touch and form a sort of network across the system. In order to get an estimate for the typical thickness of the individual branches of this network, we use a measure, sometimes called chord-length distribution [33]. The

idea is to draw lines parallel to ⟨100⟩-directions across the specimen and to color the line differently when it is inside phase A or inside phase B. The statistics of the segment (or chord) lengths, D, of a given color is then the chord length distribution $G(D)$. Figure 4 shows the chord length distribution of the precipitate phase for $c_A = 0.2$ and the two cases: no misfit and $\delta = 1\%$. The time evolution is strikingly different for both cases. While for $\delta = 0\%$ the chord length distribution exhibits a maximum shifting towards larger values of D, $G(D)$ remains more or less static for $\delta = 1.0\%$ with a strong maximum. The chord length distribution includes information on both, the size distribution of the precipitates and their shape. For example, $G(D)$ would be a delta function for the case of cubic precipitates of the same size, while for any distribution of spheres $G(D)$ decreases monotonically. The maximum of $G(D)$ in the case of no misfit (Fig. 4a) is therefore due to some flattening of the interfaces perpendicularly to the ⟨100⟩-directions. While the shift of the maximum of $G(D)$ to the right for $\delta = 0\%$ indicates some coarsening, the position of the maximum at $D \approx$ two lattice parameters is independent of time for $\delta = 1\%$. This means that the thickness of typical domains remains of the order of only several lattice spacing, despite the fact that a percolated network of such domains covers the whole system. Using the "natural scaling method" proposed in Ref. [34], we also tested the scaling behavior of the data without misfit. Except for small values of the scaled variable $D/\bar{D}$, data obtained after 4000 MCS can be well fitted by a scaling curve $\bar{G}$, which is different for the two concentrations $c_A = 0.1$ and $c_A = 0.2$ (Fig. 5).

IV. CONCLUSION

In the present paper with have investigated the effect of internal stresses caused by a lattice misfit between precipitates and matrix on the precipitate size distribution by meaus of Monte Carlo simulations. Our conclusions of these investigations are as follows:

- The scaled precipitate size distribution, $g(\rho)$ was found to be broader in comparison to the prediction from the LSW-theory for all lattice misfits δ. This is presumably due

to the basic assumption in the LSW-theory of zero volume fraction of the precipitate phase [6].

- We observed a further broadening of $g(\rho)$ in cases of large misfit. This result is in disagreement with theoretical considerations, which predicted a narrowing of $g(\rho)$ as the consequence of an inverse coarsening process [19], but agrees with numerical solutions of an extended Cahn-Hilliard equation, which considers elastic interactions [22].

- We believe that this broadening of $g(\rho)$ is due to the strong anisotropy in the system with elastic interactions. The shape of the precipitates are significantly elongated and they are oriented along the elastically soft $\langle 100 \rangle$-directions. This anisotropy in shape and orientation favors coalescence of neighboring precipitates.

These results have been obtained for a model that contains numerous simplifications. Due to the long range nature of elastic interactions, the simulations become very time consuming and cannot be extended to very large precipitate sizes. In addition, one has to be aware of finite size effects caused by the small system size [35]. The model does not allow for dislocations, for example misfit dislocations appearing in real alloys at the interface between the phases. The model also does not consider ordering in the precipitates, such as in the γ' phase in nickel-base superalloys, where anti-phase boundaries can hinder the coalescence of neighboring precipitates [36,37]. Finally, the elastic constants between precipitates and matrix are assumed identical, which is not the case in many alloys. Since all these effects may lead to quite different morphologies of the two-phase mixture [15,22], one must, therefore, be vary careful in generalizing experimental and computational results on precipitate size distributions in alloys, where elastic interactions cannot be completely excluded.

Acknowledgments

The work of H. Gupta and J. L. Lebowitz was supported by NSF Grant DMR-9813268, and AFOSR Grant F49620-98-1-0207.

REFERENCES

[1] Wagner, R.; and Kampmann, R.: in: P. Haasen (ed.), Materials Science and Technology. Vol 5, Chap. 4, VCH Verlagsges., Weinheim (1991).

[2] Binder, K.: in: P. Haasen (ed.), Materials Science and Technology, Vol 5, Chap. 7, VCH Verlagsges., Weinheim (1991).

[3] Gunton, J. D.; San Miguel, M.; Sahni, P. S.: in: C. Domb and J.L. Lebowitz (eds.). Phase Transitions and Critical Phenomena, Vol. 8, Academic Press, New York (1983).

[4] Lifshitz, I. M.; Slyozov V.V.: J. Phys. Chem. Solids 19 (1961) 35.

[5] Wagner, C.: Z. Elektrochem. 65 (1961) 581.

[6] Voorhees, P. W.: J. Stat. Phys. 38 (1985) 231.

[7] Akaiwa, N.; Voorhees, P. W.: Phys. Rev. E 49 (1994) 3860.

[8] Voorhees, P. W.; Glicksman, M. E.: Acta Metall. 32 (1984) 2001; ibid. 32 (1984) 2013.

[9] Marqusee, J. A; Ross J.: J. Chem. Phys. 80 (1984) 536.

[10] Enomoto, Y.; Kawasaki, K.; Tokuyama, M.: Acta Metall. 35 (1987) 907.

[11] Marder, M.: Phys. Rev. Lett. 55 (1985) 2953.

[12] Brailsford, A. D.; Wynblatt, P.: Acta Metall. 27 (1979) 489.

[13] Alkemper, J.; Snyder, V.A.; Akaiwa, N.; Voorhees, P. W.: Phys. Rev. Lett. 82 (1999) 2725; Snyder, V.A.; Alkemper, J.; Voorhees, P.W.: Acta Mater. 48 (2000) 2689.

[14] Laraia, V. J.; Johnson W. C.; Voorhees, P. W.: Scripta Metall. 23 (1989) 1749.

[15] Fratzl, P.; Penrose, O.; Lebowitz, J. L.: J. Stat. Phys. 95 (1999) 1429.

[16] Paris, O.; Langmayr, F.; Vogl, G.; Fratzl, P.: Z. Metallk. 86 (1995) 860.

[17] P. Fratzl P.; Penrose, O.: Acta Metall. Mater. 43 (1995) 2921; Fratzl, P.; Penrose, O.:

Acta Mater. 44 (1996) 3227.

[18] Gupta, H.; Weinkamer, R.; Fratzl, P.; Lebowitz, J. L.: submitted to Acta Mater.

[19] Miyazaki, T.; Koyama, T.: Mat. Sci. Eng. A169 (1993) 159.

[20] Su, C. H.; Voorhees, P. W.: Acta Mater. 44 (1996) 1987.

[21] Miyazaki, T.; Doi, M.: Mat. Sci. Eng. A110 (1989) 175.

[22] Orlikowski, D.; Sagui, C.; Somoza, A.; Roland, C.: Phys. Rev. B 59 (1999) 8646.

[23] Laberge, C. A.; Fratzl, R.; Lebowitz, J. L.: Phys. Rev. Lett. 75 (1995) 4448; Laberge, C. A.; Fratzl, P.; Lebowitz, J. L.: Acta Mater. 45 (1997) 3949.

[24] Weinkamer, R.; Gupta, H.; Fratzl, P.; Lebowitz, J. L.: to appear in Europhys. Lett.

[25] Khachaturyan, A. G.: Soviet Phys. Crystallogr. 10 (1965) 248.

[26] Cook, H. E.; DeFontaine, D.: Acta Metall. 17 (1969) 915.

[27] Khachaturyan, A. G.: Theory of Structural Transformations in Solids, Wiley, New York (1983).

[28] Dederichs, P.H.; Schober, H.: in: Landolt-Börnstein III/13a, Springer, Berlin (1981).

[29] Binder, K.; Heermann, D. W.: Monte Carlo Simulation in Statistical Physics - An Introduction, Springer, Berlin (1988).

[30] Stauffer, D.: Introduction to Percolation Theory, Taylor & Francis, London/Philadelphia (1985).

[31] Hayward, S.; Heermann, D. W.; Binder, K.: J. Stat. Phys. 49 (1987) 1053.

[32] Binder, K: Solid State Comm. 34 (1980) 191.

[33] Porod, G.: in: O. Glatter and O. Kratky (eds.), Small Angle X-ray Scattering, Academic Press, London/New York (1982).

[34] Fratzl, P.; Lebowitz, J. L.; Marro, J.; Kalos, M.H.: Acta Metall. 31 (1983) 1849.

[35] Heermann, D. W.; Yixue, L.; Binder, K.: Physica A 230 (1996) 132.

[36] Nielaba, P.; Fratzl, P.; Lebowitz, J. L.: J. Stat. Phys. 95 (1999) 23.

[37] Rubin, G.; Khachaturyan, A. G.: Acta Mater. 47 (1999) 1995.

FIGURES

FIG. 1. "X-ray transmission micrographs" of the system showing the precipitate morphology for different lattice misfit δ and $c_A = 0.2$ at $t = 6000$ MCS; no lattice misfit, $\delta = 0\%$ (left), $\delta = 0.5\%$ (middle), $\delta = 1\%$ (right). Bright regions indicate a high intensity of solute A atoms.

FIG. 2. Time evolution of the size of the largest cluster, n_{max}, (given as percentage of all A atoms) for different lattice misfits and two concentrations, $c_A = 0.1$ (left), and $c_A = 0.2$, (right). Data points are connected by straight lines to improve the readability. Note the different scales on the y-axes.

FIG. 3. Scaled precipitate size distributions, $g(\rho)$, for various misfits and $c_A = 0.1$; $\rho \equiv R/\bar{R}$. Error bars, plotted only for the case of no misfit and largest misfit ($\delta = 1\%$), mark the standard deviation of the mean. Data points are connected by straight lines. The dashed line corresponds to the scaled precipitate size distribution predicted by the LSW-theory as it would look like in this representation.

FIG. 4. Chord length distribution, $G(D)$, (see text) for $c_A = 0.2$ plotted at six different times for misfits $\delta = 0\%$ (top) and $\delta = 1\%$ (bottom). Curves drawn are guides to the eyes only.

FIG. 5. Scaled chord length distribution $\bar{G}$ (see text) for $c_A = 0.1$ (open symbols) and $c_A = 0.2$ (full symbols) and no misfit obtained with the "natural scaling method" proposed in Ref. [34]. Data for 4000 MCS (circles), 5000 MCS (triangles) and 6000 MCS (squares) is included. The curves connect data at the latest time for $c_A = 0.1$ (black line) and $c_A = 0.2$ (gray line).

FIG. 1

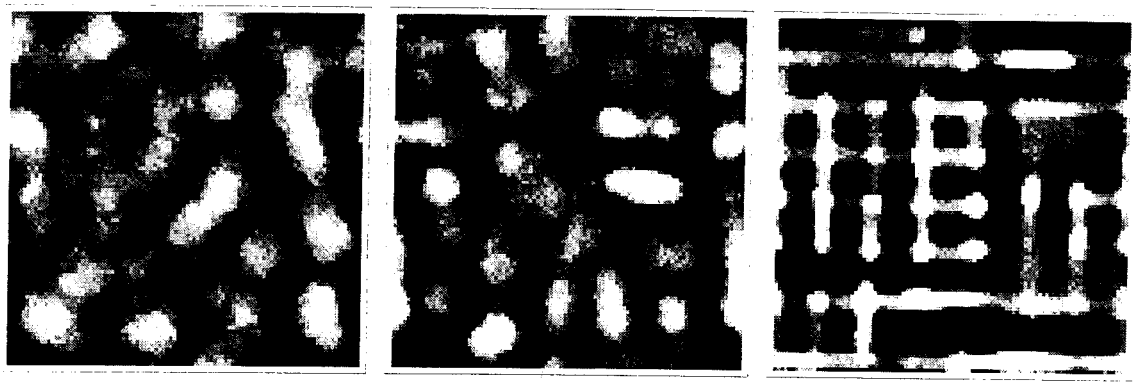

FIG. 2

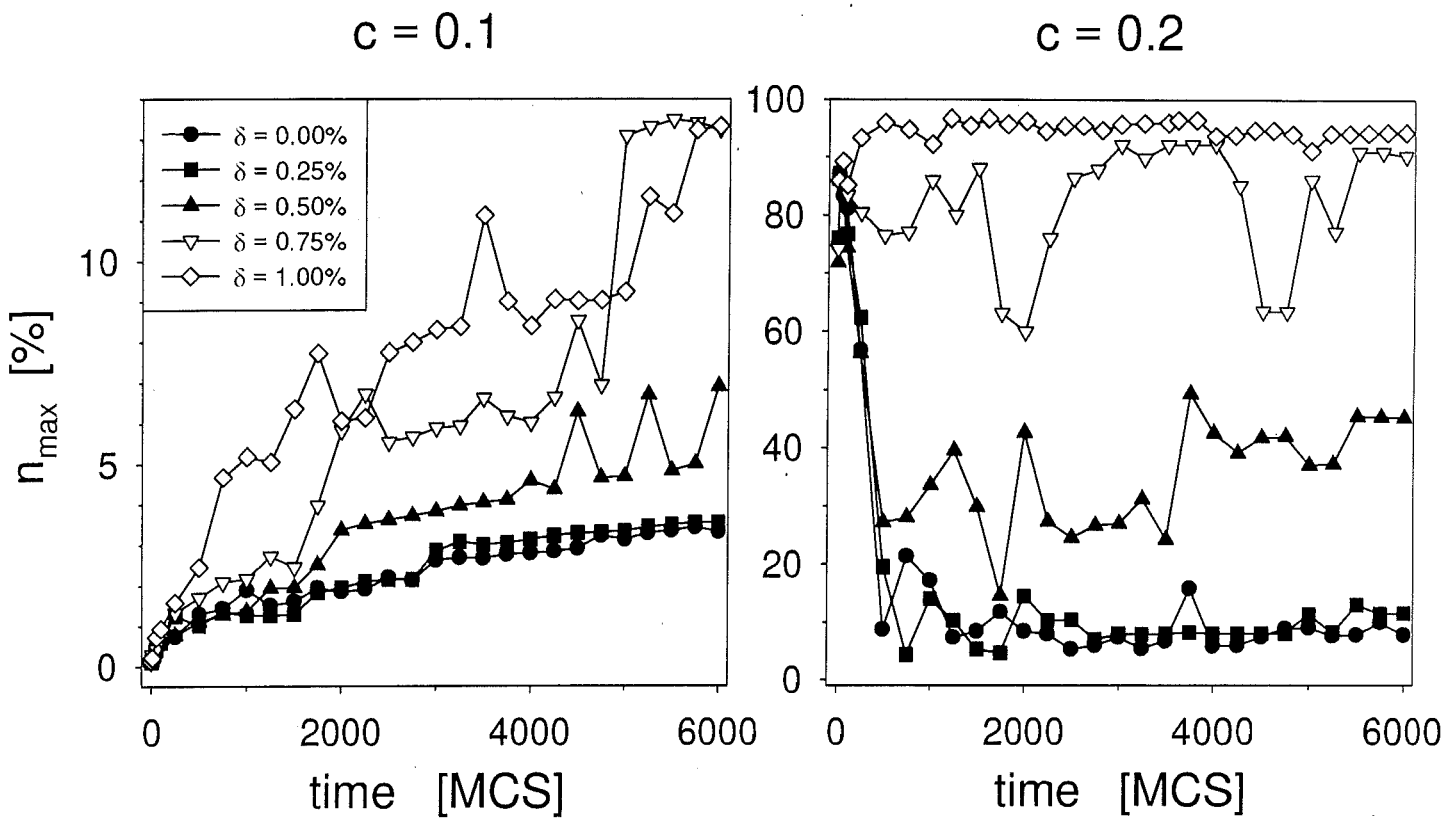
c = 0.1
c = 0.2
δ = 0.00%
δ = 0.25%
δ = 0.50%
δ = 0.75%
δ = 1.00%
η_{max} [%]
0
5
10
0
20
40
60
80
100
0
2000
4000
6000
time [MCS]
time [MCS]

FIG. 3

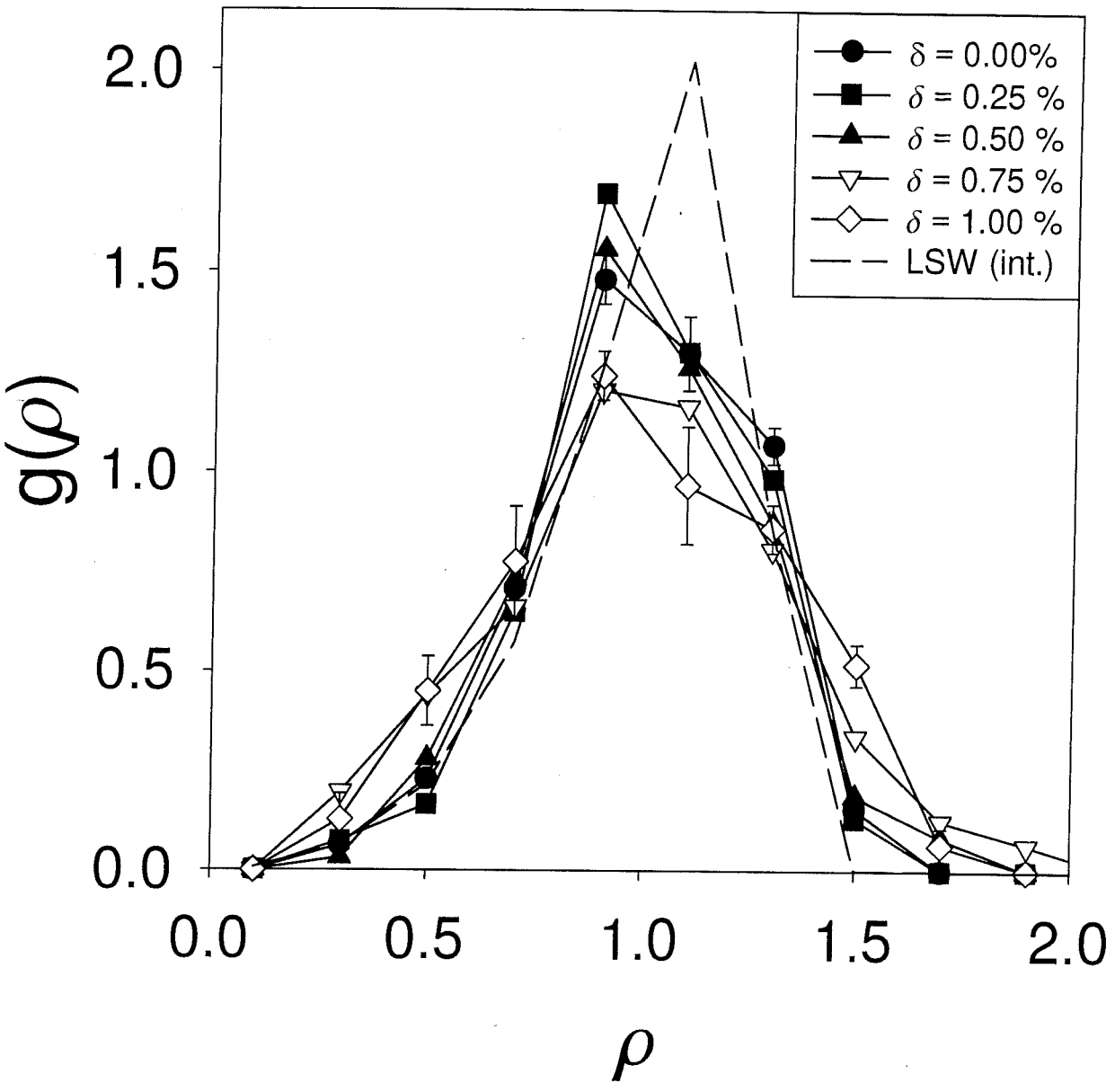

FIG. 4

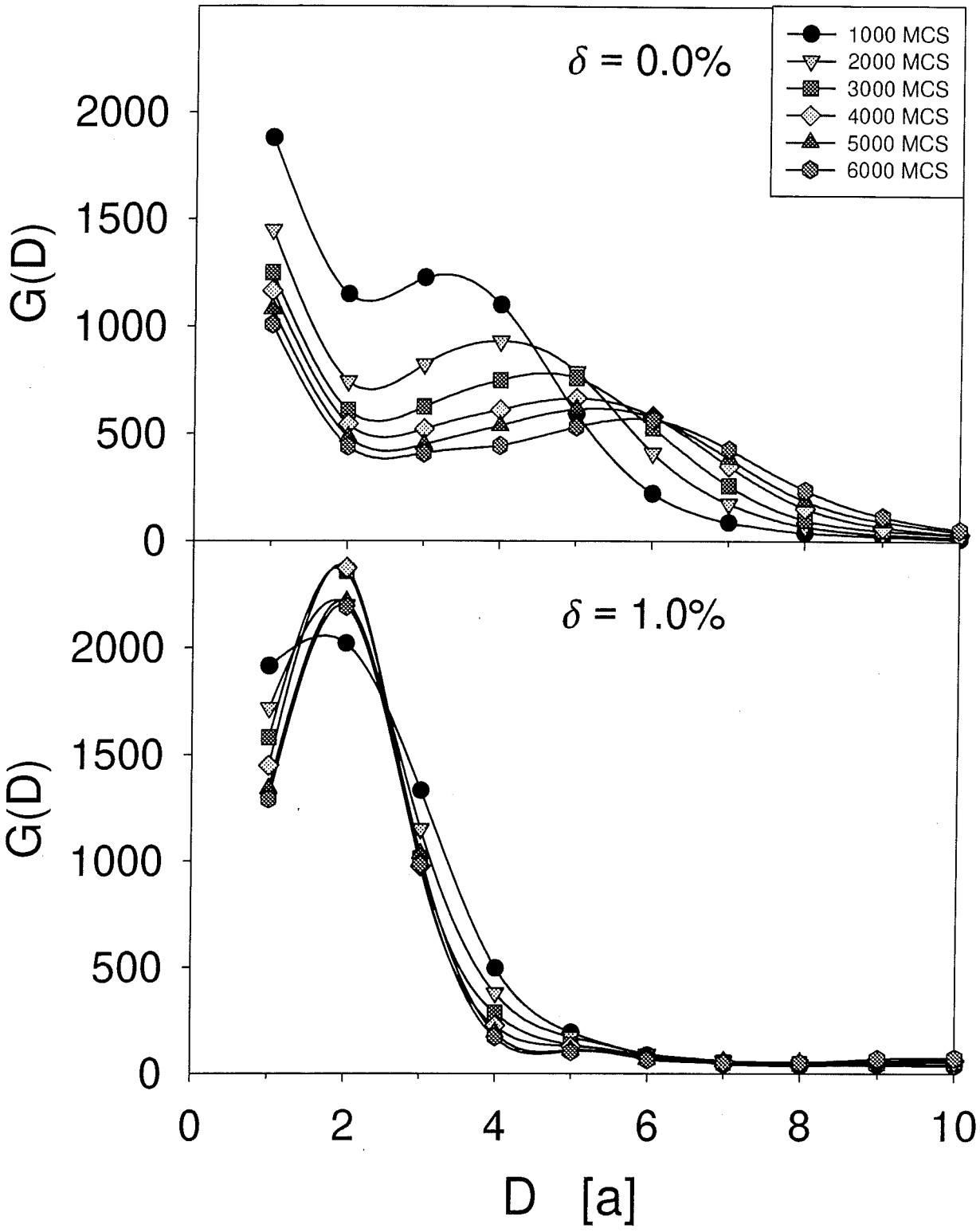
δ = 0.0%
1000 MCS
2000 MCS
3000 MCS
4000 MCS
5000 MCS
6000 MCS
G(D)
2000
1500
1000
500
0
δ = 1.0%
G(D)
2000
1500
1000
500
0
0
2
4
6
8
10
D [a]

FIG. 5